



Elimination of copper obstacle factor in anaerobic digestion effluent for value-added utilization: Performance and resistance mechanisms of indigenous bacterial consortium

Zhiqiang Gu ^a, Hongbin Yan ^a, Qi Zhang ^{a,*}, Yunpu Wang ^a, Cuixia Liu ^b, Xian Cui ^a, Yuhuan Liu ^a, Zhigang Yu ^c, Xiaodan Wu ^a, Roger Ruan ^d

^a State Key Laboratory of Food Science and Resources, Engineering Research Center for Biomass Conversion, Ministry of Education, Nanchang University, Nanchang, Jiangxi 330047, PR China

^b School of Energy & Environment, Zhongyuan University of Technology, Zhengzhou 450007, PR China

^c Australian Centre for Water and Environmental Biotechnology (formerly AWMC), The University of Queensland, Brisbane, QLD 4072, Australia

^d Center for Biorefining and Department of Bioproducts and Biosystems Engineering, University of Minnesota, Saint Paul 55108, USA

ARTICLE INFO

Keywords:

Anaerobic digestion effluent
Copper
Indigenous bacterial consortium
Extracellular polymeric substances
Metagenomics

ABSTRACT

The presence of excessive residual Cu(II), a high-risk heavy metal with potential toxicity and biomagnification property, substantially impede the value-added utilization of anaerobic digestion effluent (ADE). This study adapted indigenous bacterial consortium (IBCs) to eliminate Cu(II) from ADE, and their performances and resistance mechanisms against Cu(II) were analyzed. Results demonstrated that when the Cu(II) exposure concentration exceeded 7.5 mg/L, the biomass of IBCs decreased significantly, cells produced a substantial amount of ROS and EPS, at which time the intracellular Cu(II) content gradually decreased, while Cu(II) accumulation within the EPS substantially increased. The combined features of a high PN/PS ratio, a reversed Zeta potential gradient, and abundant functional groups within EPS collectively render EPS a primary diffusion barrier against Cu(II) toxicity. Mutual physiological and metagenomics analyses reveal that EPS synthesis and secretion, efflux, DNA repair along with coordination between each other were the primary resistance mechanisms of IBCs against Cu(II) toxicity. Furthermore, IBCs exhibited enhanced resistance by enriching bacteria carrying relevant resistance genes. Continuous pretreatment of actual ADE with IBCs at a 10-day hydraulic retention time (HRT) efficiently eliminated Cu(II) concentration from 5.01 mg/L to ~0.68 mg/L by day 2. This elimination remained stable for the following 8 days of operation, further validated their good Cu(II) elimination stability. Notably, supplementing IBCs with 200 mg/L polymerized ferrous sulfate significantly enhanced their settling performance. By elucidating the intricate interplay of Cu(II) toxicity and IBC resistance mechanisms, this study provides a theoretical foundation for eliminating heavy metal barriers in ADE treatment.

1. Introduction

Intensified concentrated animal feeding operations (CAFOs) offer enhanced production efficiency and profitability while consuming fewer resources. However, the agricultural non-point source pollution resulting from the substantial livestock manure has become increasingly prominent (Hu et al., 2017). Anaerobic digestion offers a compelling solution for the sustainable and safe management of livestock manure, transforming it into valuable resources while mitigating environmental risks (Chew et al., 2021). Despite its effectiveness, anaerobic digestion generates a substantial volume of anaerobic digestion effluent (ADE),

posing a significant management challenge. Inappropriate disposal and utilization of ADE often lead to secondary environmental contamination (Yang et al., 2022). The 14th Five-Year Plan for Cleaner Production (2021–2025) issued by China's National Development and Reform Commission emphasizes that by 2025, the comprehensive resource utilization rate of livestock manure will exceed 80%.

Advanced treatment and value-added utilization of ADE can not only help prevent environmental pollution but also recycle valuable resources such as organic matter and nutrients (Zeng et al., 2022). Currently, the value-added utilization of ADE mainly involves the following methods: (i) serving as a medium for cultivating microalgae to

* Corresponding author.

E-mail address: zhangqi09300218@163.com (Q. Zhang).

generate biomass for the production of biodiesel or animal feed (Almomani et al., 2023); (ii) functioning as a liquid fertilizer for land irrigation, effectively enhancing nitrogen absorption by plants, boosting crop yield, and improving the soil structure (Zeng et al., 2022); (iii) being used for seeds soaking to expedite germination, promote growth, prevent diseases, strengthen seedlings, and enhance yield (Zhao et al., 2014); (iv) serving as a feed additive to boost animal resistance, enhance the breeding environment, and improve the nutritional value of feed (Li et al., 2022).

Nonetheless, significant barriers exist for the efficient utilization of ADE. For instance, certain trace elements, such as copper, are commonly employed as additives to enhance the growth and immunity of livestock in CAFOs. However, only 20%–30% of metal ions undergo absorption and metabolic processes, with the remainder being excreted from the body (Li and Zhu, 2023). Furthermore, on cattle farms, hoof baths constitute one of the most vital measures for preventing and mitigating hoof diseases. The primary component of the hoof solution used is 4%–8% copper sulfate, resulting in the presence of residual copper sulfate in the manure. Consequently, copper enters livestock manure either directly or indirectly. Anaerobic digestion, which was ineffective in significantly reducing copper concentration, resulted in a substantial accumulation of copper in ADE, with concentrations ranging from 4.7 to 59.4 mg/L (Zeng et al., 2021). Copper is essential as a micronutrient, but it can become toxic when it exceeds a certain threshold level for all living organisms (Yin et al., 2019). For example, excessive copper accumulation can disrupt plant physiological metabolism, damage plant cell structure and impede photosynthesis (Yang et al., 2022a). Additionally, copper possesses the property of biomagnification, leading to its accumulation through food chains, which is considered a risk for human beings (Thanigaivel et al., 2023). To achieve the safe treatment and enhanced utilization of ADE, it is imperative to eliminate copper from ADE.

Currently, various traditional techniques, including adsorption, flocculation, chemical precipitation, ion exchange, and supercritical fluid extraction, have been extensively researched and employed for copper elimination (Guan et al., 2022; Wang et al., 2023a; Wang and You, 2023). Although these methods are effective in eliminating copper, they come with limitations, including resource-intensive processes, time-consuming procedures, and the potential risk of secondary pollution (Sarker et al., 2023). So far, cost-effective method for eliminating copper from ADE has not been identified. Bioremediation techniques are considered promising for remediating polluted environments by utilizing organisms to detoxify heavy metals from their hazardous forms to less harmful states (Song et al., 2022). Bioremediation can be accomplished with the assistance of various living organisms, such as algae, bacteria, fungi, and plants (Guo et al., 2021). Among these, bacteria are widely recognized for their bioremediation effectiveness, attributed to the adaptability and versatility of these microorganisms (Sreedevi et al., 2022). Bacterial bioremediation is primarily characterized by processes like bioaccumulation, biosorption, biomineratization, bioleaching, bioprecipitation, and redox reactions (Sreedevi et al., 2022). Bacterial heavy metal ions uptake capacities varies widely, typically ranging from 1 to 500 mg/g (Yin et al., 2019).

Generally, a single bacterium often exhibits limited tolerance to heavy metals, requiring long-term domestication prior to application, and it is primarily effective against a narrow range of heavy metals (Lin et al., 2022). Conversely, indigenous bacterial consortium (IBCs) isolated from heavy metal-contaminated sites can alleviate the metabolic burden of individual chassis cells, diminish the excessive buildup and toxicity of intermediate metabolites, and exhibit heightened adaptability and robustness in intricate environmental conditions (Liu et al., 2017). Importantly, for survival in harsh heavy metal-contaminated environments, IBCs have evolved specific resistance mechanisms and intricate intracellular pathways to utilize, interact with, adapt to, and detoxify heavy metals, promoting cellular regeneration (de Alencar et al., 2017). Consequently, IBCs exhibit resilience to elevated

concentrations of heavy metals and can efficiently tackle complex heavy metal remediation tasks. In our previous studies, IBCs isolated from swine farm wastewater exhibited significant detoxification and turbidity reduction capabilities, which could decrease the COD and TP in ADE from 3034 to 20.80 mg/L to 672.20 and 14.50 mg/L, respectively, along with a decrease in turbidity from 89.74 NTU to 50.68 NTU, and *Chlorella vulgaris* could grow in it successfully after pretreatment (Gu et al., 2021). Therefore, to alleviate the heavy metal barrier factor in ADE prior to its value-added utilization, this study further explored the pretreatment effectiveness of isolated IBCs on copper, a representative heavy metal contamination.

In this study, we investigated the physiological responses of IBCs to Cu(II) toxicity to elucidate potential resistance mechanisms. Subsequently, we aimed to investigate how IBCs resist and eliminate Cu(II) from the perspective of the variations in the contribution of EPS in content and composition, as well as the profiles of bacterial communities and functional genes. Furthermore, to demonstrate the practical and economic feasibility of IBCs, we pretreated actual ADE under continuous mode to evaluate their capacity to eliminate Cu(II) and other contaminants. Additionally, the separation of bacteria sludge and effluent by iron-based flocculants was conducted to facilitate the value-added utilization of ADE. These results may contribute to the development of a cost-effective and sustainable technology for copper bioremediation in ADE.

2. Materials and methods

2.1. Chemicals and IBCs

Chemical agents were Analytical Reagents, purchased from Sino-pharm Chemical Reagent Co., Ltd (Shanghai, China). The Cu(II) stock solution was prepared by dissolving copper sulfate ($\text{CuSO}_4 \cdot 5\text{H}_2\text{O}$) in ultrapure water, resulting in a final concentration of 1000 mg/L. Subsequently, it was diluted to the required concentration for use.

This study utilized IBCs previously described by Gu et al. (2021), with details on specific bacterial strains and proportions provided in Text S1. The IBCs were stored at -80°C . Upon activation, the strains were cultured in an enrichment medium (Table S1) at 28°C under continuous illumination of 3500 Lux. Cells were collected by centrifugation at 8000 rpm for 10 min, followed by three washes with deionized water to obtain a bacterial sludge for subsequent experiments.

2.2. Exposure of IBCs to Cu(II)

A 9-day exposure experiment was conducted to explore the effect of Cu(II) on IBCs. 300 mL of sterilized synthetic ADE containing varying Cu (II) concentrations (121°C , 20 min) was added to each 500 mL conical flask. Cu(II) exposure concentrations were established at 0, 2.5, 5.0, 7.5, 10.0, 15.0, 20.0 and 40.0 mg/L, and the corresponding groups were denoted as Cu0, Cu2.5, Cu5, Cu7.5, Cu10, Cu15, Cu20 and Cu40, respectively. Three parallel controls were set up for each group of experiments. The sterilized synthetic ADE characteristics were as follows: total organic carbon (TOC) at 1962.20 mg/L, ammonium ($\text{NH}_4^+\text{-N}$) at 296.20 mg/L, total phosphate (TP) at 210.90 mg/L, and Zeta potential at -11.85 mV (Details are provided in Table S2). All flasks were inoculated with a bacterial sludge concentration of 1 g/L (wet weight) and manually shaken three times daily. The cultivation conditions were adopted as described in Section 2.1. Bacterial growth (dry weight), oxidative stress parameters [i.e., reactive oxygen species (ROS), superoxide dismutase (SOD) and cell viability (Live/Dead)], and physicochemical parameters of the wastewater, including nutrients (e.g., carbon, nitrogen and phosphorus), pH, dissolved oxygen (DO), Zeta potential, and Cu (II) content were determined according to methods described in Text S2-S6. Additionally, the amount of Cu(II) adsorbed by EPS and bacterial cells was determined (Refer to Text S6 for details). The IBCs were examined using a Scanning Electron Microscope (SEM, Regulus8100,

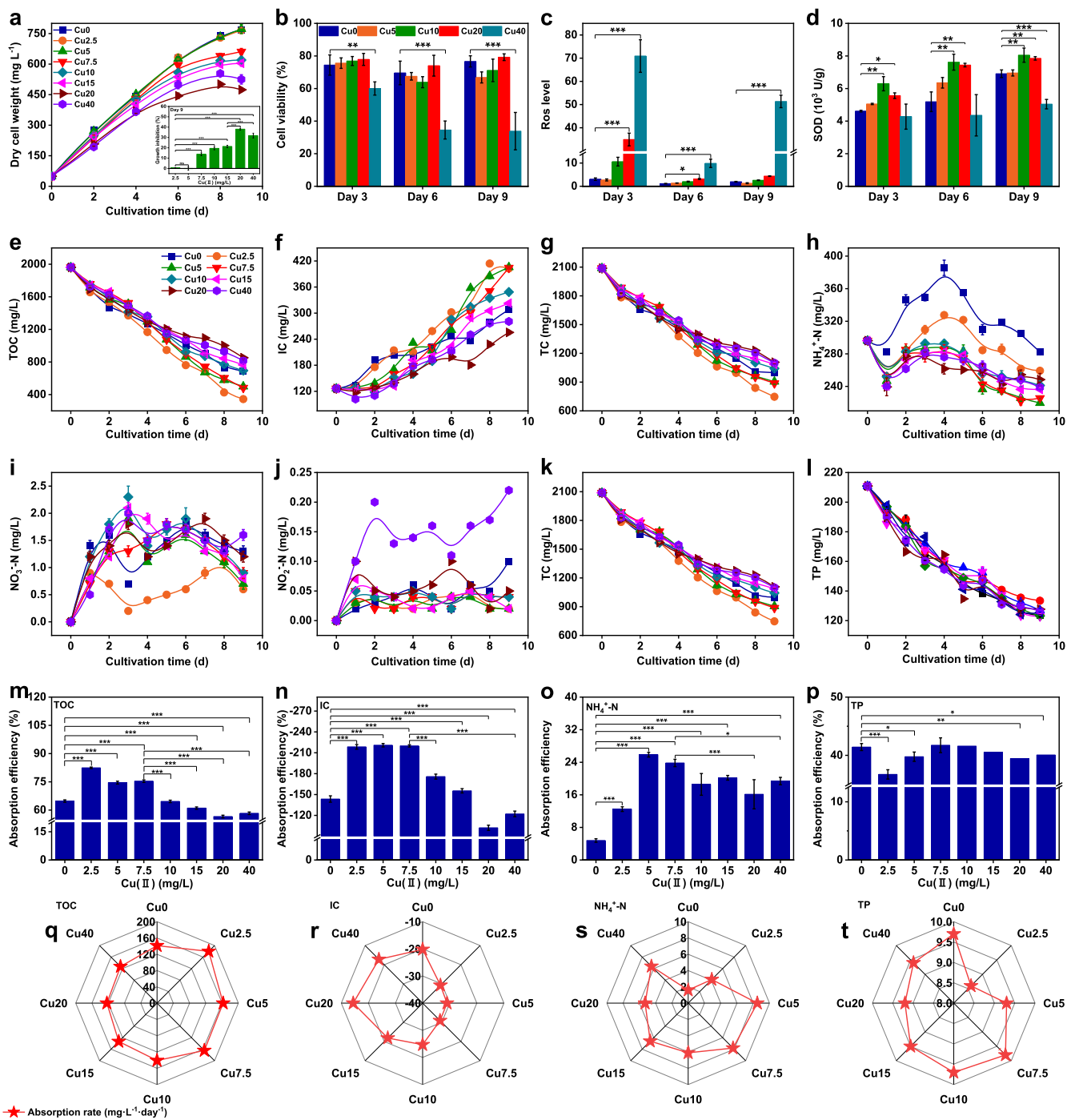


Fig. 1. The effect of Cu(II) on bacterial growth and nutrient absorption. Dry cell weight (DCW) and growth inhibition of IBCs on day 9 (a); cell viability (b); ROS levels (c); SOD activities (d); concentration variation of nutrients (e–i); absorption efficiency (m–p), and absorption rate (q–t) of TOC, IC, NH_4^+ -N and TP.

Hitachi High-Technologies, Japan), and a Transmission Electron Microscope (TEM, JEM-2100, JEOL, Japan) to obtain images of the morphology, EPS secretions and elemental distribution (Details are provided in Text S7).

2.3. EPS extraction and characterization

The bacterial sludge samples collected on day 9 were analyzed for the EPS composition, with a focus on the stratified distribution of loosely bound EPS (LB-EPS) and tightly bound EPS (TB-EPS). EPS extraction was conducted employing a modified thermal method (Zhang et al., 2016). Protein (PN) and polysaccharide (PS) content in EPS samples were

quantified by the Lowry-Folin and Phenol-sulfuric acid methods, respectively, using bovine serum albumin (BSA) and glucose as standards (Wang et al., 2023b). The Zeta potential of LB-EPS, TB-EPS, bacterial cells with EPS and bacterial cells without EPS was also determined following the method as described in Text S5. To characterize the composition and optical properties of EPS, a suite of spectroscopic techniques was employed. UV-vis spectra were acquired using a UV-Visible spectrophotometer (UV-9000, Metash, China). Functional group analysis of lyophilized EPS was performed with a Fourier transform infrared spectrometer (FTIR, Nicolet iS50, LingLu, China). Three-dimensional excitation-emission matrix fluorescence spectroscopy (3D-EEM) on the spectrometer (FLS 1000, Edinburgh, United

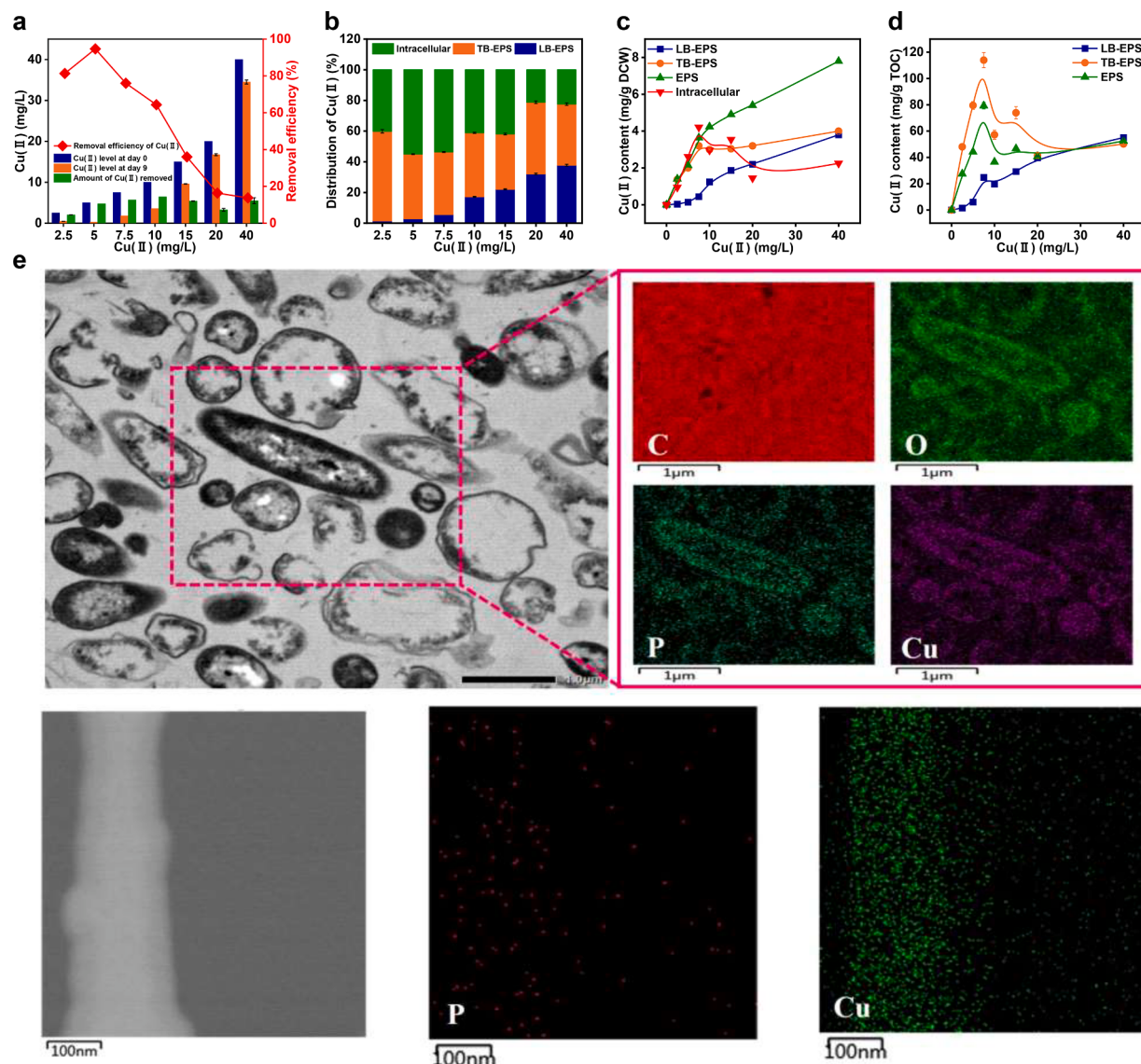


Fig. 2. Effect of Cu(II) concentrations on Cu(II) elimination by IBCs. Cu(II) elimination by IBCs (a); Cu(II) distribution in IBCs (DCW refers to the dry cell weight of IBCs, specifically representing the Cu(II) content of each component per unit of dry cell weight) (b, c); Cu(II) distribution in EPS (TOC refers to EPS concentration, specifically representing the Cu(II) content of each component per unit of EPS concentration) (d); TEM analysis with elemental mapping of IBCs exposed to 40 mg/L Cu(II) (e).

Kingdom) revealed information about fluorescent organics within the EPS. Detailed steps for EPS extraction and characterization are presented in Text S8-S9.

2.4. Metagenome sequencing analysis

Biological triplicate samples from Cu(II) exposure groups (Cu5 and Cu40) and the control group (Cu0) were collected and stored at -80°C for subsequent metagenomic sequence analysis. Genomic DNA was extracted from cells using a DNA Extraction Kit (D5625-01, Omega Biotech, America) and sequenced on an Illumina Nova 6000 platform at Majorbio (Shanghai Majorbio Bio-Pharm Technology Co., Ltd., China) following procedures such as fragmentation, library construction, and bridge PCR. Detailed information on sample preparation, DNA extraction, fragmentation, PE library construction, Bridge PCR, metagenomic sequencing, and sequence analysis can be found in Text S10. The raw metagenomic sequence data have been deposited in the NCBI Sequence Read Archive (SAR) with accession number PRJNA1007406.

2.5. Continuous treatment of actual ADE by IBCs and bacterial sludge flocculation test

In the continuous experiment, 10 L of sterilized actual ADE, pre-treated with 8-layer gauze (16 mesh) filtration and centrifugation (121°C , 20 min), was introduced into a self-designed photobioreactor (PBR) with a 20 L volume (Fig. S1). The characteristics of ADE are shown in Table S3. Prior to PBR start-up, it was inoculated with a bacterial sludge concentration of 2 g/L (wet weight). The hydraulic retention time (HRT) of PBR was set to 10 days, with the total operation lasting 10 days. The cultivation conditions were adopted in Section 2.1. Nutrient concentrations, along with those of Cu(II) and Zn(II), were monitored following the methods described in Section 2.2.

On the 10th day of the continuous treatment experiment, two iron-based flocculants, ferric chloride ($\text{FeCl}_3 \cdot 6\text{H}_2\text{O}$) and polymerized ferrous sulfate (PFS2, Fe \geq 21%, Macklin), were chosen to evaluate their flocculation efficiency on IBCs. Briefly, bacterial cultures from the PBR outlet were transferred to graduated colorimetric tubes (each with a height of 12.90 cm and a diameter of 22 mm, Fig. 8e) for a 30-minute

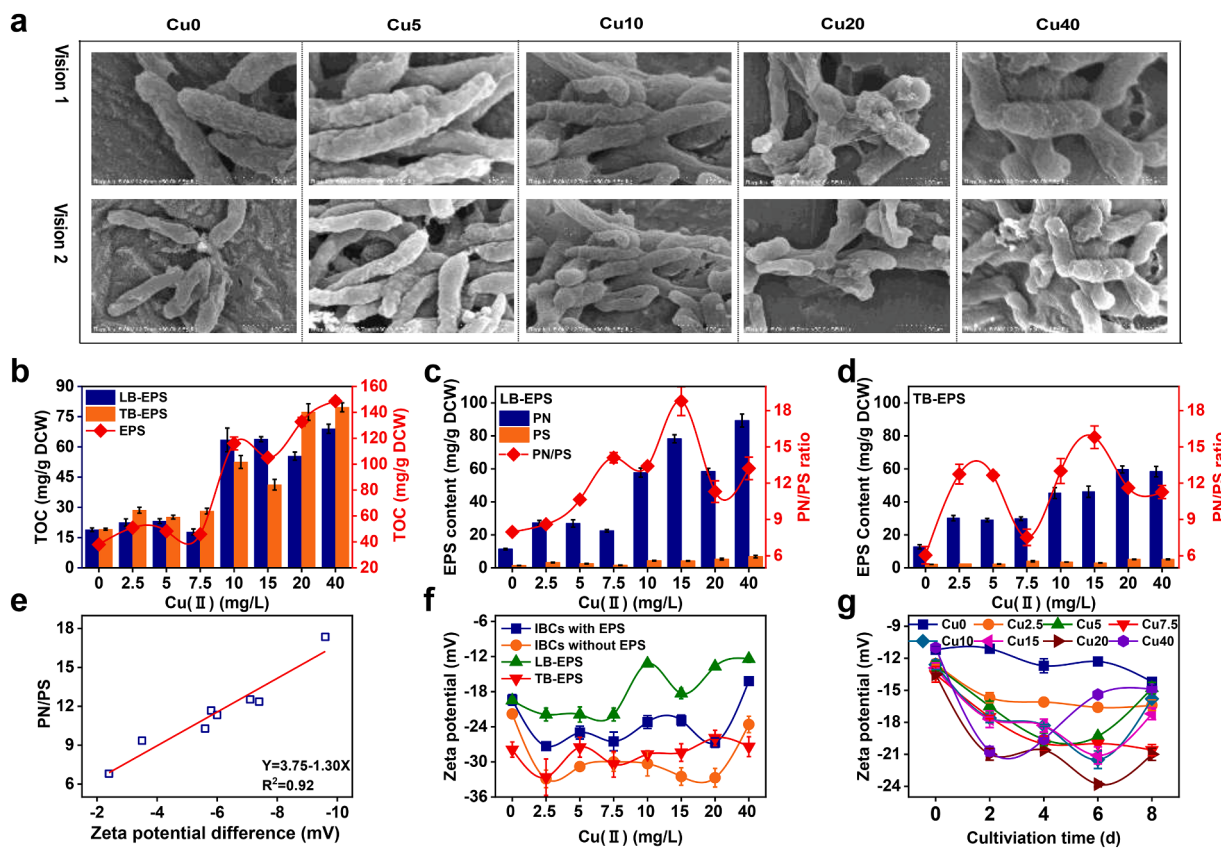


Fig. 3. The effect of Cu(II) concentration on EPS composition and content. SEM images of IBCs (a); EPS content and composition (b); PN and PS content and PN/PS ratio in EPS (c, d); the relationship between Zeta potential difference (i.e., the difference value between bacterial cells with EPS and bacterial cells without EPS) and PN/PS ratio of EPS (e); Zeta potential of LB-EPS, TB-EPS, bacterial cells with EPS and bacterial cells without EPS (f); Zeta potential of wastewater at different Cu(II) concentrations (g).

settling period. $\text{FeCl}_3 \cdot 6\text{H}_2\text{O}$ added concentrations were set at 97, 242.5, 485, 727.5, 970, and 1455 mg/L, while PFS2 added concentrations were set at 10, 20, 50, 100, 200, and 300 mg/L. The settling interface height was measured at 5-minute intervals. The sludge volume index at 30 min (SVI_{30}) was determined using standard methods (Rice et al., 2012). Following the flocculation tests, the residual Fe concentration in the supernatant of each tube was also measured following the method as described in Text S6.

2.6. Statistical analysis

Experimental data are presented as means \pm SD, and the figures were drawn using Origin 2023 (OriginLab, America). Statistical analysis was performed by one-way analysis of variance (ANOVA) followed by least significant difference (LSD) or two-tailed Student's *t*-test. Differences were considered significant at $P < 0.05$, denoted as * $P < 0.05$, ** $P < 0.01$ and *** $P < 0.001$. Data analysis was conducted using SPSS statistical software (SPSS version 23.0, SPSS Inc.).

3. Results and discussion

3.1. Physiological responses of IBCs to Cu(II) toxicity

Fig. 1a illustrates that low concentrations of Cu(II) ($\leq 5 \text{ mg/L}$) had a negligible effect on the growth of IBCs but significantly promoted the uptake of TOC and NH_4^+ -N by IBCs (**Fig. 1m and 1o**). As the Cu(II) concentration further increased, the dry weight of bacterial cells gradually declined. On day 9, Cu15, Cu20 and Cu40 exhibited relative growth inhibition rates of 21.31%, 38.03% and 31.76%, respectively (**Fig. 1a**). Moreover, With the elevation of Cu(II) concentration, the

absorption efficiency of TOC and NH_4^+ -N, as well as the production efficiency of IC, exhibited a declining trend (**Fig. 1m–1o**). Yin et al. (2019) demonstrated that the excessive uptake of Cu(II) poses significant risks to microorganisms, causing damage to cell membranes, inhibiting enzyme activity, damaging DNA, and interfering with cellular functions. The Live/Dead ratio visually indicated a significant decrease in cell viability by 19.35%, 50.35%, and 55.85% in Cu40 on days 3, 6, and 9, respectively ($P < 0.01$) (**Fig. 1b**), suggesting substantial cell damage and apoptosis following 9 days of exposure to 40 mg/L Cu(II). Forouzan et al. (2020) reported that copper induces cellular toxicity by displacing other metals in enzymes or protein complexes, resulting in the production of ROS, protein denaturation, and damage to membrane integrity. This study shows that Cu(II) exposure induced obvious oxidative stress, as evidenced by a 10.38-fold and 23.12-fold increase in ROS levels ($P < 0.001$) in Cu20 and Cu40 compared to Cu0 on day 3 (**Fig. 1c**). Noteworthy, the ROS level of bacteria exposed to 40 mg/L Cu(II) on day 9 remained significantly elevated compared to Cu0 ($P < 0.001$). As the first line of defense for direct clearance of ROS (Yang et al., 2022b), SOD activities increased with rising ROS levels (**Fig. 1d**). Notably, the SOD activity of bacteria in Cu40 did not increase in response to a sharp increase in ROS. This potentially reflects severe intracellular antioxidant system damage due to high Cu(II) toxicity (Zhou et al., 2019).

3.2. Cu(II) elimination by IBCs and its distribution

This study investigated the removal efficiency of Cu(II) by IBCs (**Fig. 2a**). At Cu(II) concentrations of 2.5 and 5.0 mg/L, after 9 days of cultivation, residual Cu(II) in wastewater decreased to $\sim 0.50 \text{ mg/L}$, meeting the agricultural irrigation water standard of China (GB 5084–2021).

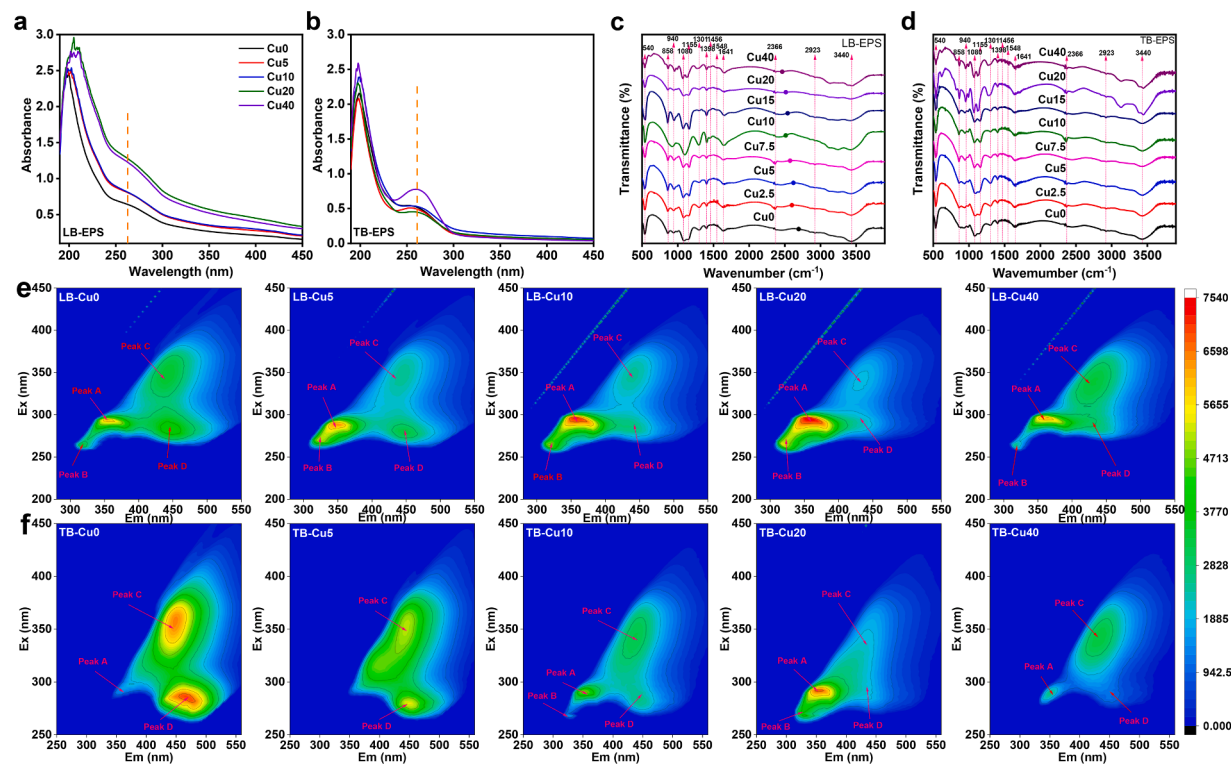


Fig. 4. UV–vis absorbance spectra for LB-EPS and TB-EPS (a, b); FTIR spectra for LB-EPS and TB-EPS (c, d); 3D-EEM spectra for LB-EPS and TB-EPS (e, f).

The distribution of Cu(II) was also investigated, specifically in EPS and intracellular compartments (Fig. 2b–2d). As the Cu(II) concentration increased from 0 to 7.5 mg/L, intracellular Cu(II) content exhibited a significant increase, reaching 4.21 mg/g. Subsequently, it decreased from 4.21 to 2.25 mg/g as the Cu(II) concentration further increased from 7.5 to 40 mg/L (Fig. 2c). With the increase in Cu(II) concentration, the Cu(II) content in TB-EPS initially increased, followed by a decrease, and eventually stabilized. Conversely, in LB-EPS, the Cu(II) content continuously increased (Fig. 2d). TEM mapping further supports this finding, as reflected that abundant Cu(II) were evenly distributed on the bacterial surface in the Cu40 sample, while significantly less was observed intracellularly (Fig. 2e). Additionally, we observed that TB-EPS predominantly adsorbing Cu(II) at low Cu(II) concentrations and saturating at higher levels. Conversely, at higher concentrations, LB-EPS played a primary role in Cu(II) adsorption (Fig. 2d). The results indicate that, at low concentrations of Cu(II), IBCs actively absorbed and accumulated Cu(II) within the cells, supporting normal growth (Forouzan et al., 2020). However, high Cu(II) concentrations suppressed cell growth and nutrient uptake, leading to increased oxidative stress (Fig. 1). At this point, IBCs shifted their strategy from active intracellular accumulation to extracellular sequestration. This involved enhanced copper efflux and increased EPS production for extracellular sequestration.

3.3. Cu(II) promoted IBCs to secrete EPS for cellular protection

Based on the results in Section 3.2, a large amount of Cu(II) was found to bind EPS under high Cu(II) concentrations. Subsequently, we further investigated the EPS secretion by IBCs. SEM visualization of IBCs morphology reveals that the cell surface of bacteria exposed to Cu(II) (especially at 20 and 40 mg/L) exhibited severe wrinkling and was surrounded by an abundant gel-like matrix, likely composed of EPS layers (Fig. 3a). This observation suggests that Cu(II) exposure triggered a significant increase in EPS secretion by IBCs, as evidenced by Fig. 3b. Specifically, the highest contents of LB-EPS and TB-EPS were observed

in Cu40, increasing by 265.17% and 316.26% compared to Cu0, respectively ($P < 0.01$). The augmentation in EPS secretion represents a self-protective mechanism employed by microorganisms to counteract external adverse effects, such as heavy metals and toxic organic compounds (Xie et al., 2020). Notably, the protein content of both LB-EPS and TB-EPS increased markedly upon Cu(II) exposure, as reflected by the elevated PN/PS ratio shown in Fig. 3c, 3d. Qian et al. (2023) identified a substantial portion of EPS composed of proteins rich in negatively charged side chains like glutamate and aspartate, which effectively bind positively charged metal ions. Dai et al. (2019) also found that, in response to Cu(II) stress, bacteria can protect themselves by secreting more proteins, and a higher PN/PS ratio can significantly increase the hydrophobicity of EPS and enhance its affinity with Cu(II). Interestingly, a linear positive correlation was observed between the Zeta potential difference and the PN/PS ratio (Fig. 3e). This suggests that the protein-rich EPS, with its higher PN/PS ratio, exhibits a more negative Zeta potential. Fig. 3f supports this conclusion, LB-EPS exhibits the lowest Zeta potential, followed by bacterial cells with EPS, TB-EPS, and bacterial cells without EPS in general. This “reversed Zeta potential gradient” creates an electrostatic barrier around the bacteria, potentially hindering the direct passage of positively charged Cu(II) through the EPS and limiting their entry into the cell. The adsorption of heavy metal ions by EPS is energy independent and non-metabolic, which is driven by the electrostatic interaction between heavy metal cations and the negative charged functional groups of EPS (Mahto et al., 2022). This is supported by changes in the Zeta potential of TB-EPS, and LB-EPS (Fig. 3f). As shown in Fig. 3g, Cu(II) exposure groups exhibit significantly lower Zeta potentials compared to that of control, further supporting the role of EPS in Cu(II) sequestration through electrostatic interactions.

3.4. EPS as the first diffusion barrier of defense against Cu(II) toxicity

Our findings demonstrate that EPS serves as a potent diffusion barrier, significantly hindering the infiltration of Cu(II) into the bacterial

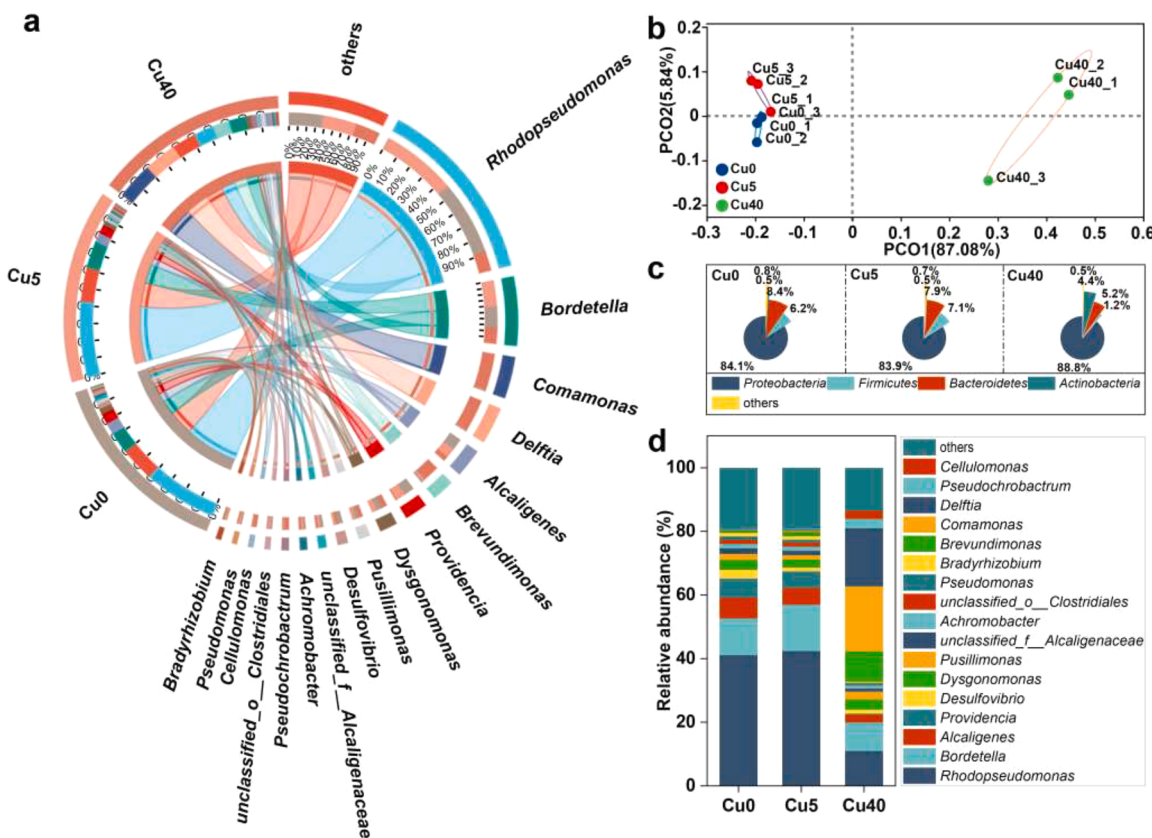


Fig. 5. Structure of microbial community. Microbial diversity at the genus level based on Circos diagram (a); PCoA analysis based on bacterial community at the genus level (b); the taxonomic compositions of the microbial community at the phylum level (c) and genus level (d).

cells. Therefore, we proceeded with further characterization of EPS. The UV-vis absorbance spectra for LB-EPS and TB-EPS exhibited similarity (Fig. 4a, 4b). An apparent peak at 260 nm was observed, attributed to aromatic rings (Yu et al., 2023). The presence of abundant aromatic structures within proteins and humic substances enables the effective binding of heavy metal ions to EPS (Wei et al., 2017).

FT-IR analysis shows the striking similarity in the peak positions between LB-EPS and TB-EPS (Fig. 4c, 4d). Key peaks included O-H of carbohydrates ($3446\text{--}3421\text{ cm}^{-1}$), N-H of proteins ($2925\text{--}2917\text{ cm}^{-1}$), C=O of amide I ($1641\text{--}1635\text{ cm}^{-1}$), N-H of amide II ($1464\text{--}1455\text{ cm}^{-1}$), carboxyl group ($1405\text{--}1398\text{ cm}^{-1}$), C-H of amide III ($1159\text{--}1135\text{ cm}^{-1}$), C-O-C of polysaccharide ($1097\text{--}1070\text{ cm}^{-1}$), and phosphate group ($865\text{--}860\text{ cm}^{-1}$) (Details are provided in Table S4) (Li et al., 2023; Xi et al., 2022; Yan et al., 2021), suggesting that the two had similar chemical compositions. The presence of hydroxyl, carboxyl group, amine and phosphorus group in EPS facilitates efficient accumulation of heavy metal ions [e.g., Cu(II) and Cd(II)], and this protects the microorganisms from heavy metal toxicity by preventing the ions from entering the intracellular environment (Yin et al., 2019). The amide II band, identified as the distinctive peak for glutathione (Li et al., 2019). Glutathione efficiently binds Cu(II), forming a stable complex that precludes their entry into cells (Yin et al., 2019). For TB-EPS, shifts in peaks from approximately 1641 , 1440 and 1082 cm^{-1} in Cu40 to 1458 , 1136 and 1070 cm^{-1} , respectively, were observed (Table S4). These shifts suggest potential binding of Cu(II) to N-H of amide II, C-H of amide III, and C-O-C of the polysaccharide.

3D-EEM spectroscopy reveals distinct fluorescent components within LB-EPS (Fig. 4e, 4f). LB-EPS exhibited four peaks: peak A belonged to protein-like substances and tryptophan (282–298/336–377 nm); peak B assigned to soluble microbial byproducts (261–267/313–323 nm); peak C attributed to aromatic polysaccharide-like substances (320–366/413–461 nm); peak D associated with humic substances (269–298/

411–475 nm) (Li et al., 2023). Consistent with LB-EPS, 3D-EEM analysis of TB-EPS (Fig. 4b) reveals a similar composition of fluorescent components, primarily comprising protein-like substances and tryptophan, aromatic polysaccharide-like substances, and humic substances. These substances, rich in metal-binding functional groups, are accountable for the adsorption of metal ions by EPS (Mahto et al., 2022). It is noteworthy that the fluorescence intensity of peak A and peak B in TB-EPS and LB-EPS decreased drastically in Cu40 compared to Cu10 and Cu20 (Table S5). This is consistent with the findings of Li et al. (2018), where the fluorescence intensity of tryptophan in EPS decreased under elevated Cu(II) concentrations. The observed decrease in fluorescence intensity suggests potential complex formation between tryptophan and Cu(II), implying its protective role in mitigating Cu(II) toxicity. Notably, the fluorescence intensity of peak D associated with humic substances in TB-EPS exhibited a gradual decline with increasing Cu(II) concentration (Table S5). This observation aligns with the well-documented metal-binding capacity of humic substances, attributed to their abundance of functional groups like hydroxyl and carboxyl (Hasani Zadeh et al., 2023).

3.5. Metagenomics analysis

3.5.1. Variations in the structure and abundance of the functional microbial community

To explore the intricate interplay between microbial resistance to Cu (II) and their remediation ability, metagenomic sequencing was performed on IBCs exposed to varying Cu(II) concentrations (Cu0, Cu5, and Cu40). Circos plots and PcoA analysis at the genus level indicates a substantial shift in community structure with increasing Cu(II) stress (Fig. 5a, 5b). The results of the Simpson index, ACE and Chao1 (Table S6) show that the evenness of distribution in Cu40 was similar to that in Cu0 and Cu5. However, the species richness significantly

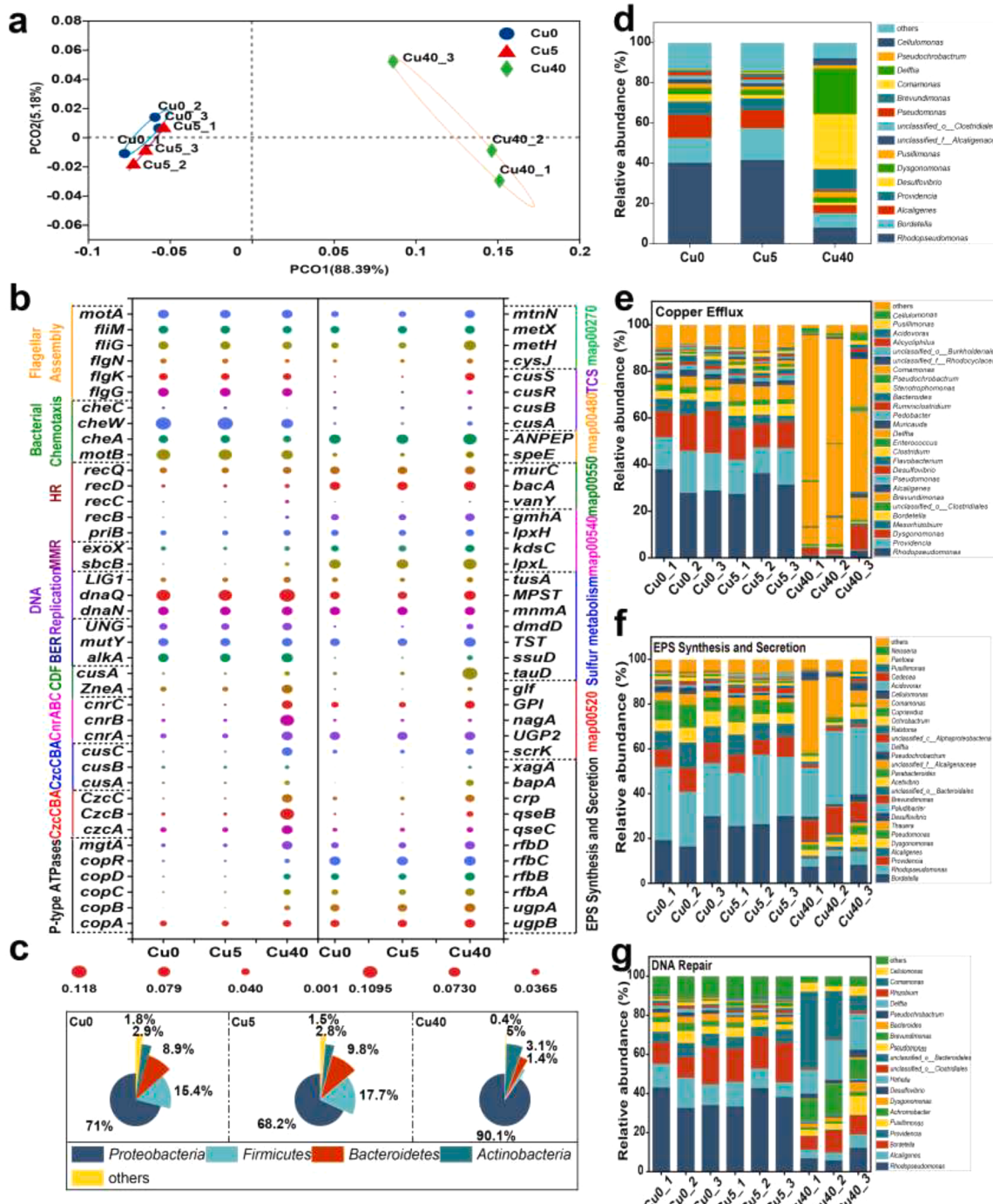


Fig. 6. PcoA analysis of functional gene composition at the KO level (a); relative abundance of detected MRGs (BER, base-excision repair; MMR, mismatch repair; HR, homologous recombination; map00520, amino sugar and nucleotide sugar metabolism; map00540, lipopolysaccharide biosynthesis; map00550, peptidoglycan biosynthesis; map00480, glutathione metabolism; TCS, two-component systems; map00270, cysteine and methionine metabolism) (b); the contribution of different key microorganisms at the phylum level (c) and genus level (d) in detected MRGs; the contribution of different key microorganisms at the genus level in the main functional genes linked to copper efflux (e), EPS synthesis and secretion (f), and DNA repair (g).

declined. Fig. 5c, 5d display the relative taxonomic abundance of bacterial communities at the phylum and genus levels. At the genus level, with an increase in Cu(II) concentration from 0 to 40 mg/L, the relative abundances of *Comamonas*, *Delftia* and *Brevundimonas* in Cu40 were 136.73, 95.95, and 14.4 times higher, respectively, than those in Cu0. This suggests their significant selective advantage and potent adaptation to Cu(II) stress.

3.5.2 Functional composition analysis based on metagenomics sequencing

When heavy metals are toxic or enriching to bacteria, the heavy metal resistance genes (MRGs) carried by the bacteria are also elevated or reduced (Lin et al., 2019). To elucidate the Cu(II) resistance mechanisms in IBCs, we functionally annotated genes using the KEGG database. PCoA analysis at the KEGG Orthology (KO) level demonstrated significant shifts in the functional gene composition of the bacterial community in Cu40 compared to Cu0 and Cu5 (Fig. 6a).

As shown in Fig. 6b, the relative abundance of genes associated with

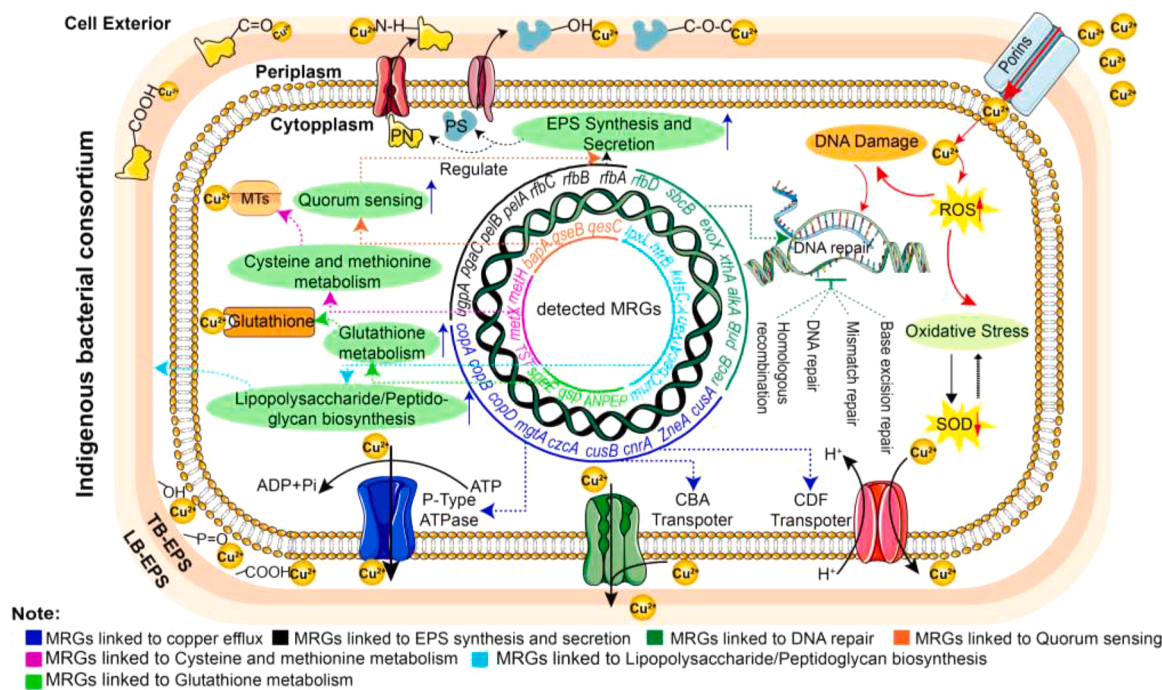


Fig. 7. The resistance mechanisms of IBCs.

EPS synthesis and secretion (e.g., *pelA*, *pgaC*, *rfaB* and *rfaD*) significantly increased in Cu40 compared to Cu0 and Cu5, suggesting enhanced EPS production potential in the Cu40 bacterial community. Notably, the relative abundance of genes involved in amino sugar and nucleotide sugar metabolism (e.g., *scrK*, *nagA* and *GPI*) also exhibited significant upregulation in Cu40, supporting the link between active sugar consumption and robust EPS production reported by Sevak et al. (2021) due to the high demand for nucleotide sugars in repetitive unit assembly, transmembrane translocation, and polymerization of EPS. It was observed that the relative abundance of genes related to sulfur metabolism (e.g., *tauD*, *ssuD*, *TST* and *MPST*) were significantly up-regulated in Cu40 compared to Cu0 ($P < 0.05$), suggesting an enhanced potential for sulphide production. A moderate release of sulphide can efficiently decrease the environmental metal concentration to permissible limits by lowering the solubility of metal-sulphide complex (Pal et al., 2022). As the first sites of cell and Cu(II) interaction, the cell wall possesses numerous anionic functional groups, including hydroxyl, carboxyl, and phosphate groups, which serve to prevent the entrance of heavy metal ions into the intracellular environment through extracellular metal sequestration (Pal et al., 2022). Notably, the relative abundance of genes involved in building major cell wall components, such as lipopolysaccharide biosynthesis (e.g., *lpX*, *htrB* and *kdsc*) and peptidoglycan biosynthesis (*vanY*, *bacA*, *murC*), showed a substantial increase in relative abundance in Cu40. Upon exposure to high concentrations of heavy metals, ions can transport along the concentration gradient and accumulate within cells (Pal et al., 2022). Efflux, a crucial defense strategy employed by numerous bacteria, emerges as a highly effective method for combating heavy metal toxicity. This potent strategy relies on diverse protein families, such as CBA (capsule biogenesis/assembly) transporters, CDF (cation diffusion facilitator) transporters, and P-type ATPases (Sevak et al., 2021). It was observed that the relative abundance of genes linked to the CBA transporter (e.g., *czcA*, *cusA* and *cnrA*), CDF transporter (i.e., *ZneA* and *cusA*) and P-type ATPases (e.g., *copA*, *copB* and *copD*) significantly increased in Cu40 compared to Cu0 and Cu5. This suggests that IBCs employ active transport mechanisms to efflux Cu(II) from the cytoplasm under Cu(II) toxicity. Specifically, the P_{1B}-ATPase (CopA) encoded by *CopA* serves as the primary conduit for intracellular copper efflux. CopA transports Cu(II) from the cytoplasm to

the periplasm and interacts with the transmembrane CusCAB pore system, encoded by *CusA* and *CusB*, to transport excess Cu(II) outside the cell (Sheldon and Skaar, 2019). Additionally, CopA and CopC, encoded by *CopA* and *CopC*, are periplasmic proteins that bind copper. They can bind 11 and 1 copper atoms on the same polypeptide, respectively, and the activation of transporters results in the accumulation of copper in the periplasmic space, protecting the cell from the toxic effects of copper (Sigel et al., 2013). Upon entering cells, another mechanism employed by cells to prevent elevated toxic copper levels involves chelation of copper through metal ion binding proteins such as cysteine-rich proteins (metallothioneins, MTs) and glutathione within the cytoplasm, binding the metal (Bazzi et al., 2020). This strategy aligns with our findings of that the relative abundance of many genes related to cysteine and methionine metabolism (e.g., *metH*, *metX* and *TST*) and glutathione metabolism (e.g., *speE*, *ANPEP* and *gsp*) was significantly upregulated in Cu40, suggesting this chelation mechanism plays a key role in copper tolerance.

Exposure to 40 mg/L Cu(II) induced evident oxidative stress in IBCs (Fig. 1c, 1d), potentially leading to severe DNA damage (Yin et al., 2019). It prompted the activation of various DNA repair pathways as a defensive response. This is substantiated by these highly abundant genes mainly involved in DNA replication (i.e., *dnaN*, *dnaQ* and *LIG1*), mismatch repair (e.g., *sbcB* and *exoX*), base excision repair (e.g., *xthA*, *tag* and *alkA*) and homologous recombination (e.g., *priB*, *recB* and *recC*). Additionally, signaling proteins recruit various signaling pathways, including the two-component system (TCS), which serves as a bridge between external environmental stimuli and specific adaptive response mechanism (Pal et al., 2022). The relative abundance of *cusA*, *cusB*, *cusR*, and *cusS*, which encode TCS was significantly up-regulated in Cu40, primarily regulating copper homeostasis (Huang et al., 2019). Chemotaxis is a process by which motile prokaryotic organisms move towards attractant gradients or away from repellents (Sevak et al., 2021). Cu(II) exposure significantly suppressed bacterial chemotaxis and motility, as a bacterial stress response evidenced by down-regulated the relative abundance of many bacterial chemotaxis-related genes (e.g., *motA*, *cheA*, *cheC*, and *fliG*). Table S7 provides detailed information on the relative abundance of detected MRGs associated with copper tolerance in IBCs.

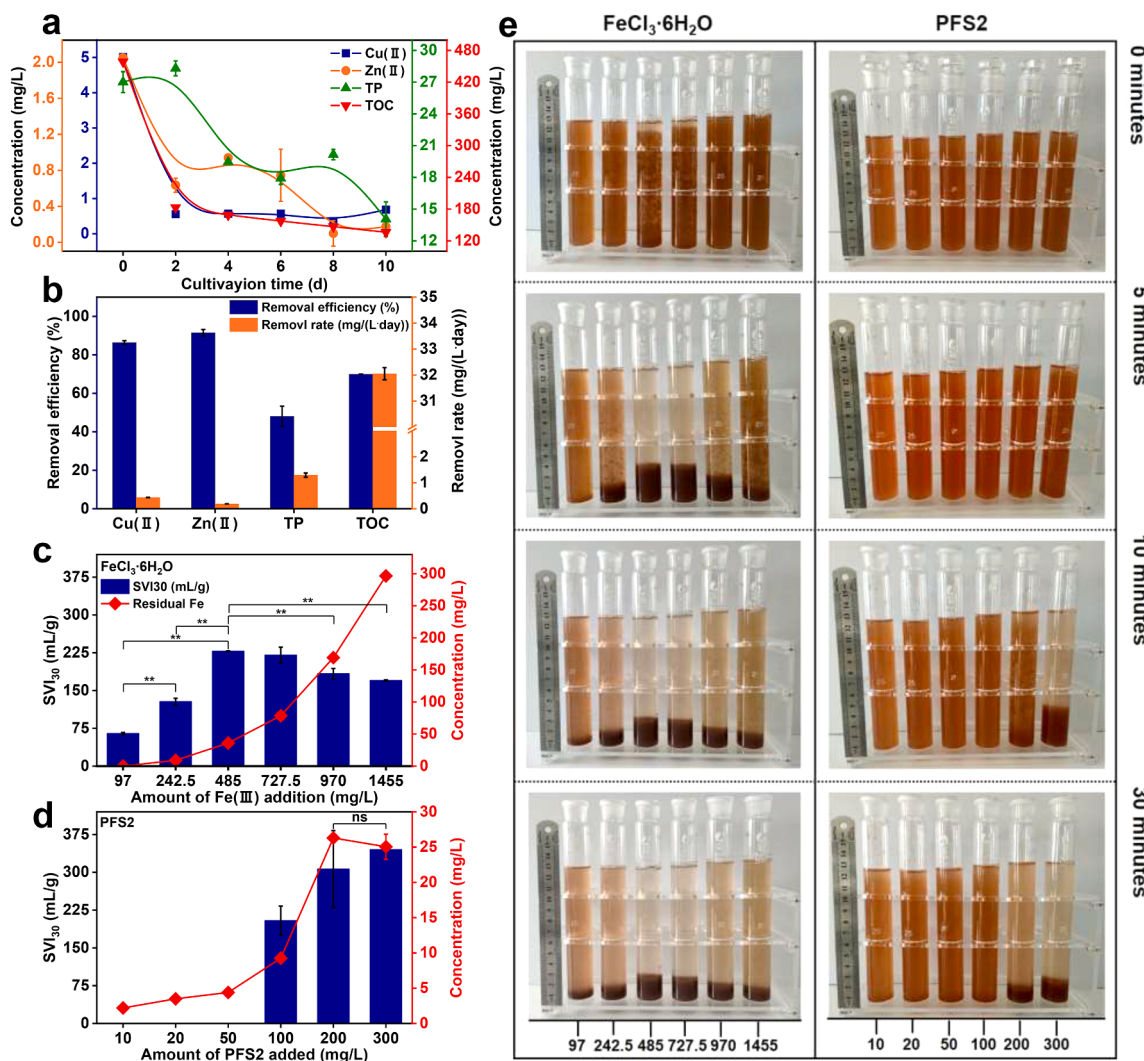


Fig. 8. Concentration variation of pollutants during continuous pretreatment (a); elimination effect of pollutants in effluent (b); SVI₃₀ of IBCs and Fe concentrations in the supernatant after adding FeCl₃·6H₂O (c) and PFS2 (d); images of sludge sedimentation at different phases (0, 5, 10 and 30 min) (e).

Furthermore, we conducted an in-depth analysis of bacterial contributions to detected MRGs at both the phylum and genus levels. At the phylum level, the predominant contributors to detected MRGs in the bacterial community in Cu40 were *Proteobacteria* and *Actinobacteria* (Fig. 6c). The shift in the composition of detected MRGs contributors was correlated with alterations in bacterial abundance (Fig. 5d), providing additional evidence that IBCs enhanced their copper resistance by enriching bacteria carrying resistance genes. Considering the crucial roles of microbial interactions in shaping the structure of microbial communities, a network analysis of the co-occurrence was constructed. Notably, Fig. S3 reveals that positive interactions were more prevalent than negative interactions, suggesting coordination among IBCs in response to high Cu(II) toxicity. This further demonstrates the superior ability of the isolated IBCs in eliminating Cu(II). Fig. 6e–6g shows that *Brevundimonas*, *Comamonas* and *Delftia* were the predominant contributors to detected MRGs associated with copper efflux, EPS synthesis and secretion, and DNA repair in Cu40 (Fig. 7). These bacteria can be selectively screened to reconstruct the dominant bacterial consortium, thereby augmenting the elimination of Cu(II) from ADE.

3.6. Employing IBCs for the continuous pretreatment of actual ADE

To further validate the efficacy of IBCs in pretreating ADE containing heavy metal, we pretreated actual ADE in the continuous mode. Fig. 8a,

8b reveals a rapid decline in effluent Cu(II) concentration to ~0.6 mg/L within just 2 days of continuous treatment, meeting the standard for agricultural irrigation water in China (GB 5084–2021). Notably, the Cu (II) concentration remained relatively stable throughout the subsequent 8 days of operation, indicating that IBCs have good Cu(II) elimination stability and can effectively eliminate Cu(II) under continuous pretreatment. Simultaneously, the removal rates of influent Zn(II), TP, and TOC were 91.50%, 48.05%, and 69.94%, respectively, indicating that IBCs have strong overall capabilities in achieving efficient ADE pretreatment. However, the self-sedimentation effect of IBCs was suboptimal (Fig. S3). Despite the transfer of heavy metal ions to IBCs, their elimination from ADE did not occur, posing significant challenges for subsequent applications. Notably, two iron-based flocculants exhibited a significant flocculation effect on IBCs. Fig. 8c illustrates the most exceptional settling ability (SVI₃₀ of 228.01 mL/g) observed in the 485 mg/L FeCl₃·6H₂O group, with a residual iron concentration of 36 mg/L in the supernatant. However, the excessive addition of FeCl₃·6H₂O resulted in the turbidity of the wastewater supernatant (Fig. 8e). With the addition of 200 mg/L PFS2 for 30 min, the SVI₃₀ of IBCs and residual iron concentration in wastewater were determined to be 306.31 mL/g and 26.30 mg/L, respectively (Fig. 8d). This dosage proved to be the optimal amount for achieving an ideal separation between bacteria and effluent. Additionally, iron is a vital micronutrient for plant growth. A judicious increment in iron supply enhances the photosynthetic rate of

phytoplankton, consequently reducing CO₂ and macronutrient levels (Rana and Prajapati, 2021).

4. Conclusion

Elevated Cu(II) concentrations significantly inhibited the growth of IBCs and induced the activation of antioxidant defense system in IBCs. Stimulated by high concentrations of Cu(II), IBCs exhibited enhanced EPS secretion. Simultaneously, intracellular Cu(II) content gradually declined, while its content in LB-EPS exhibited a continuous upward trend. Cells secreted EPS rich in proteins, exhibiting strong Cu(II) binding affinity. The strong affinity of EPS for Cu(II) can be attributed to its richness in negatively charged functional groups, like hydroxyl, amine, and carboxyl groups. Under Cu(II) stress, metagenomic analysis revealed that bacteria carrying MRGs were selectively enriched in IBCs, where these genes were mainly involved in copper efflux, EPS synthesis and secretion, and DNA repair. Additionally, IBCs exhibit excellent overall performance, efficiently eliminating heavy metals and organic matter from actual ADE in continuous treatment. In the effluent of continuous treatment, the addition of 200 mg/L PFS2 resulted in an SVI₃₀ of 306.31 mL/g for the bacterial sludge, facilitating the efficient separation of IBCs and ADE, thus benefiting the subsequent value-added utilization of ADE.

Data availability

Data will be made available on request.

CRediT authorship contribution statement

Zhiqiang Gu: Conceptualization, Methodology, Investigation, Formal analysis, Data curation, Writing – original draft. **Hongbin Yan:** Investigation, Conceptualization, Supervision. **Qi Zhang:** Conceptualization, Methodology, Formal analysis, Resources, Writing – review & editing. **Yunpu Wang:** Investigation, Formal analysis. **Cuixia Liu:** Investigation, Data curation, Visualization. **Xian Cui:** Conceptualization, Supervision, Writing – review & editing. **Yuhuan Liu:** Conceptualization, Writing – review & editing. **Zhigang Yu:** Investigation, Formal analysis. **Xiaodan Wu:** Conceptualization, Supervision. **Roger Ruan:** Formal analysis, Writing – review & editing.

Declaration of competing interest

The authors declare that they have no known competing financial interests or personal relationships that could have appeared to influence the work reported in this paper.

Acknowledgments

This work was supported by the National Natural Science Foundation of China (No. 22106062, No. 2216026), Major Discipline Academic and Technical Leaders Training Program of Jiangxi Province (No. 20225BCJ23026), Natural Science Foundation of Chongqing (2022NSCQ-MSX0546, 2022NSCQ-MSX5200).

Supplementary materials

Supplementary material associated with this article can be found, in the online version, at doi:10.1016/j.watres.2024.121217.

References

- Almomani, F., Hosseinzadeh-Bandbafha, H., Aghbashlo, M., Omar, A., Joo, S.W., Vasseghian, Y., Karimi-Maleh, H., Shiung Lam, S., Tabatabaei, M., Rezania, S., 2023. Comprehensive insights into conversion of microalgae to feed, food, and biofuels: current status and key challenges towards implementation of sustainable biorefineries. *Chem. Eng. J.* 455, 140588 <https://doi.org/10.1016/j.cej.2022.140588>.
- Bazzi, W., Abou Fayad, A.G., Nasser, A., Haraoui, L.P., Dewachi, O., Abou-Sitta, G., Nguyen, V.K., Abara, A., Karah, N., Landecker, H., Knapp, C., McEvoy, M.M., Zaman, M.H., Higgins, P.G., Matar, G.M., 2020. Heavy metal toxicity in armed conflicts potentiates AMR in *A. baumannii* by selecting for antibiotic and heavy metal co-resistance mechanisms. *Front. Microbiol.* 11, 1–12. <https://doi.org/10.3389/fmicb.2020.00068>.
- Chew, K.R., Leong, H.Y., Khoo, K.S., Vo, D.V.N., Anjum, H., Chang, C.K., Show, P.L., 2021. Effects of anaerobic digestion of food waste on biogas production and environmental impacts: a review. *Environ. Chem. Lett.* 19, 2921–2939. <https://doi.org/10.1007/s10311-021-01220-z>.
- Dai, M., Zhou, G., Ng, H.Y., Zhang, J., Wang, Y., Li, N., Qi, X., Miao, M., Liu, Q., Kong, Q., 2019. Diversity evolution of functional bacteria and resistance genes (*CzcA*) in aerobic activated sludge under Cd(II) stress. *J. Environ. Manag.* 250, 109519 <https://doi.org/10.1016/j.jenvman.2019.109519>.
- de Alencar, F.L.S., Navoni, J.A., do Amaral, V.S., 2017. The use of bacterial bioremediation of metals in aquatic environments in the twenty-first century: a systematic review. *Environ. Sci. Pollut. Res.* 24, 16545–16559. <https://doi.org/10.1007/s11356-017-9129-8>.
- Forouzan, E., Karkhane, A.A., Yakhchali, B., 2020. Exploring metal resistance genes and mechanisms in copper enriched metal ore metagenome. *bioRxiv* 1–32. [doi:10.1101/2020.07.02.184564](https://doi.org/10.1101/2020.07.02.184564).
- Gu, Z., Liu, Y., Zou, G., Zhang, Q., Lu, R., Yan, H., Cao, L., Liu, T., Ruan, R., 2021. Enhancement of nutrients removal and biomass accumulation of *Chlorella vulgaris* in pig manure anaerobic digestate effluent by the pretreatment of indigenous bacteria. *Bioresour. Technol.* 328, 124846 <https://doi.org/10.1016/j.biortech.2021.124846>.
- Guan, X., Yuan, X., Zhao, Y., Wang, H., Wang, H., Bai, J., Li, Y., 2022. Application of functionalized layered double hydroxides for heavy metal removal: a review. *Sci. Total Environ.* 838, 155693 <https://doi.org/10.1016/j.scitotenv.2022.155693>.
- Guo, S., Xiao, C., Zhou, N., Chi, R., 2021. Speciation, toxicity, microbial remediation and phytoremediation of soil chromium contamination. *Environ. Chem. Lett.* 19, 1413–1431. <https://doi.org/10.1007/s10311-020-01114-6>.
- Hasani Zadeh, P., Fermoso, F.G., Collins, G., Serrano, A., Mills, S., Abram, F., 2023. Impacts of metal stress on extracellular microbial products, and potential for selective metal recovery. *Ecotoxicol. Environ. Saf.* 252, 114604 <https://doi.org/10.1016/j.ecoenv.2023.114604>.
- Hu, Y., Cheng, H., Tao, S., 2017. Environmental and human health challenges of industrial livestock and poultry farming in China and their mitigation. *Environ. Int.* 107, 111–130. <https://doi.org/10.1016/j.envint.2017.07.003>.
- Huang, N., Mao, J., Zhao, Y., Hu, M., Wang, X., 2019. Multiple transcriptional mechanisms collectively mediate copper resistance in *Cupriavidus gilardii* CR3. *Environ. Sci. Technol.* 53, 4609–4618. <https://doi.org/10.1021/acs.est.8b06787>.
- Li, H., Yao, H., Zhang, D., Zuo, L., Ren, J., Ma, J., Pei, J., Xu, Y., Yang, C., 2018. Short- and long-term effects of manganese, zinc and copper ions on nitrogen removal in nitrification-anammox process. *Chemosphere* 193, 479–488. <https://doi.org/10.1016/j.chemosphere.2017.11.002>.
- Li, J., Jiang, Z., Chen, S., Wang, T., Jiang, L., Wang, M., Wang, S., Li, Z., 2019. Biochemical changes of polysaccharides and proteins within EPS under Pb(II) stress in *Rhodotorula mucilaginosa*. *Ecotoxicol. Environ. Saf.* 174, 484–490. <https://doi.org/10.1016/j.ecoenv.2019.03.004>.
- Li, S., Zhu, L., 2023. Copper regulates degradation of typical antibiotics by microalgal-fungal consortium in simulated swine wastewater: insights into metabolic routes and dissolved organic matters. *Water Res.* 245, 120654 <https://doi.org/10.1016/j.watres.2023.120654>.
- Li, Y., Gong, S., Song, C., Tian, H., Yan, Z., Wang, S., 2023. Roles of microbial extracellular polymeric substances in corrosion and scale inhibition of circulating cooling water. *ACS EST Water* 3, 743–755. <https://doi.org/10.1021/acsestwater.2c00524>.
- Li, Y., Xu, S., Li, J., Li, S., Zhang, X., Xie, X., 2022. High-value processing and utilization for digested manure effluent treatment: advances and challenges. *Curr. Pollut. Rep.* 8, 445–455. <https://doi.org/10.1007/s40726-022-00232-9>.
- Lin, H., Wang, Z., Liu, C., Dong, Y., 2022. Technologies for removing heavy metal from contaminated soils on farmland : a review. *Chemosphere* 305, 135457. <https://doi.org/10.1016/j.chemosphere.2022.135457>.
- Lin, Y., Ye, Y., Hu, Y., Shi, H., 2019. The variation in microbial community structure under different heavy metal contamination levels in paddy soils. *Ecotoxicol. Environ. Saf.* 180, 557–564. <https://doi.org/10.1016/j.ecoenv.2019.05.057>.
- Lin, Y., Ding, M., Ling, W., Yang, Y., Zhou, X., Li, B.Z., Chen, T., Nie, Y., Wang, M., Zeng, B., Li, X., Liu, H., Sun, B., Xu, H., Zhang, J., Jiao, Y., Hou, Y., Yang, H., Xiao, S., Lin, Q., He, X., Liao, W., Jin, Z., Xie, Y., Zhang, B., Li, T., Lu, X., Li, J., Zhang, F., Wu, X.L., Song, H., Yuan, Y.J., 2017. A three-species microbial consortium for power generation. *Energy Environ. Sci.* 10, 1600–1609. <https://doi.org/10.1039/c6ee03705d>.
- Mahto, K.U., Vandana, Priyadarshane, M., Samantaray, D.P., Das, S., 2022. Bacterial biofilm and extracellular polymeric substances in the treatment of environmental pollutants: beyond the protective role in survivability. *J. Clean. Prod.* 379, 134759 <https://doi.org/10.1016/j.jclepro.2022.134759>.
- Pal, A., Bhattacharjee, S., Saha, J., Sarkar, M., Mandal, P., 2022. Bacterial survival strategies and responses under heavy metal stress: a comprehensive overview. *Crit. Rev. Microbiol.* 48, 327–355. <https://doi.org/10.1080/1040841X.2021.1970512>.
- Qian, J., Wan, T., Ye, Y., Li, J., Toda, T., Li, H., Sekine, M., Takayama, Y., Koga, S., Shao, S., Fan, L., Xu, P., Zhou, W., 2023. Insight into the formation mechanism of algal biofilm in soy sauce wastewater. *J. Clean. Prod.* 394, 136179 <https://doi.org/10.1016/j.jclepro.2023.136179>.

- Rana, M.S., Prajapati, S.K., 2021. Resolving the dilemma of iron bioavailability to microalgae for commercial sustenance. *Algal Res.* 59, 102458 <https://doi.org/10.1016/j.algal.2021.102458>.
- Rice, E.W., Baird, R.B., Eaton, A.D., Clesceri, L.S., 2012. *Standard Methods for the Examination of Water and Wastewater*. American Public Health Association, USA. ISBN 978-087553-013-0.
- Sarker, A., Al Masud, M.A., Deepo, D.M., Das, K., Nandi, R., Ansary, M.W.R., Islam, A.R.M.T., Islam, T., 2023. Biological and green remediation of heavy metal contaminated water and soils: a state-of-the-art review. *Chemosphere* 332, 138861. <https://doi.org/10.1016/j.chemosphere.2023.138861>.
- Sevak, P.I., Pushkar, B.K., Kapadne, P.N., 2021. Lead pollution and bacterial bioremediation: a review. *Environ. Chem. Lett.* 19, 4463–4488. <https://doi.org/10.1007/s10311-021-01296-7>.
- Sheldon, J.R., Skaar, E.P., 2019. Metals as phagocyte antimicrobial effectors. *Curr. Opin. Immunol.* 60, 1–9. <https://doi.org/10.1016/j.coic.2019.04.002>.
- Sigel, A., Sigel, H., Sigel, R.K.O., Banci, L., 2013. *Metal Ions in Life Sciences*. Springer. Met. Cell.
- Song, P., Xu, D., Yue, J., Ma, Y., Dong, S., Feng, J., 2022. Recent advances in soil remediation technology for heavy metal contaminated sites: a critical review. *Sci. Total Environ.* 838, 156417 <https://doi.org/10.1016/j.scitotenv.2022.156417>.
- Sreedevi, P.R., Suresh, K., Jiang, G., 2022. Bacterial bioremediation of heavy metals in wastewater: a review of processes and applications. *J. Water Process Eng.* 48, 102884 <https://doi.org/10.1016/j.jwpe.2022.102884>.
- Thanigaivel, S., Vickram, S., Dey, N., Jeyanthi, P., Subbaiya, R., Kim, W., Govarathanan, M., Karmegam, N., 2023. Ecological disturbances and abundance of anthropogenic pollutants in the aquatic ecosystem: critical review of impact assessment on the aquatic animals. *Chemosphere* 313, 137475. <https://doi.org/10.1016/j.chemosphere.2022.137475>.
- Wang, L., Cheng, W.C., Xue, Z.F., Xie, Y.X., Lv, X.J., 2023a. Feasibility study of applying electrokinetic technology coupled with enzyme-induced carbonate precipitation treatment to Cu- and Pb-contaminated loess remediation. *J. Clean. Prod.* 401, 136734 <https://doi.org/10.1016/j.jclepro.2023.136734>.
- Wang, M., You, X.Y., 2023. Efficient adsorption of antibiotics and heavy metals from aqueous solution by structural designed PSSMA-functionalized-chitosan magnetic composite. *Chem. Eng. J.* 454, 140417 <https://doi.org/10.1016/j.cej.2022.140417>.
- Wang, Z., Wang, H., Nie, Q., Ding, Y., Lei, Z., Zhang, Z., Shimizu, K., Yuan, T., 2023b. Pb (II) bioremediation using fresh algal-bacterial aerobic granular sludge and its underlying mechanisms highlighting the role of extracellular polymeric substances. *J. Hazard. Mater.* 444, 130452 <https://doi.org/10.1016/j.jhazmat.2022.130452>.
- Wei, L., Li, Y., Noguera, D.R., Zhao, N., Song, Y., Ding, J., Zhao, Q., Cui, F., 2017. Adsorption of Cu²⁺ and Zn²⁺ by extracellular polymeric substances (EPS) in different sludges: effect of EPS fractional polarity on binding mechanism. *J. Hazard. Mater.* 321, 473–483. <https://doi.org/10.1016/j.jhazmat.2016.05.016>.
- Xi, Y., Xie, T., Liu, Y., Wu, Y., Liu, H., Su, Z., 2022. Carboxymethyl cellulose stabilized ferrous sulfide @ extracellular polymeric substance for Cr (VI) removal: characterization, performance, and mechanism 425.
- Xie, Q., Liu, N., Lin, D., Qu, R., Zhou, Q., Ge, F., 2020. The complexation with proteins in extracellular polymeric substances alleviates the toxicity of Cd (II) to *Chlorella vulgaris*. *Environ. Pollut.* 263, 114102 <https://doi.org/10.1016/j.envpol.2020.114102>.
- Yan, W., Qian, T., Zhang, L., Wang, L., Zhou, Y., 2021. Interaction of perfluorooctanoic acid with extracellular polymeric substances—role of protein. *J. Hazard. Mater.* 401, 123381 <https://doi.org/10.1016/j.jhazmat.2020.123381>.
- Yang, W., Li, S., Qv, M., Dai, D., Liu, D., Wang, W., Tang, C., Zhu, L., 2022a. Microalgal cultivation for the upgraded biogas by removing CO₂, coupled with the treatment of slurry from anaerobic digestion: a review. *Bioresour. Technol.* 364, 128118 <https://doi.org/10.1016/j.biortech.2022.128118>.
- Yang, Zi, Yang, F., Liu, J.L., Wu, H.T., Yang, H., Shi, Y., Liu, J., Zhang, Y.F., Luo, Y.R., Chen, K.M., 2022b. Heavy metal transporters: functional mechanisms, regulation, and application in phytoremediation. *Sci. Total Environ.* 809, 151099 <https://doi.org/10.1016/j.scitotenv.2021.151099>.
- Yang, Z., Zhu, L., Liu, J., Cheng, Y., Waiho, K., Chen, A., Wang, Y., 2022c. Polystyrene microplastics increase Pb bioaccumulation and health damage in the Chinese mitten crab *Eriocheir sinensis*. *Sci. Total Environ.* 829, 154586 <https://doi.org/10.1016/j.scitotenv.2022.154586>.
- Yin, K., Wang, Q., Lv, M., Chen, L., 2019. Microorganism remediation strategies towards heavy metals. *Chem. Eng. J.* 360, 1553–1563. <https://doi.org/10.1016/j.cej.2018.10.226>.
- Yu, J., Xiao, K., Xu, H., Li, Y., Xue, Q., Xue, W., Zhang, A., Wen, X., Xu, G., Huang, X., 2023. Spectroscopic fingerprints profiling the polysaccharide/protein/humic architecture of stratified extracellular polymeric substances (EPS) in activated sludge. *Water Res.* 235, 119866 <https://doi.org/10.1016/j.watres.2023.119866>.
- Zeng, W., Qiu, J., Wang, D., Wu, Z., He, L., 2022. Ultrafiltration concentrated biogas slurry can reduce the organic pollution of groundwater in fertilization. *Sci. Total Environ.* 810, 151294 <https://doi.org/10.1016/j.scitotenv.2021.151294>.
- Zeng, Z., Zheng, P., Da, K., Li, Y., Li, W., Dongdong, X., Chen, W., Pan, C., 2021. The removal of copper and zinc from swine wastewater by anaerobic biological-chemical process: performance and mechanism. *J. Hazard. Mater.* 401, 123767 <https://doi.org/10.1016/j.jhazmat.2020.123767>.
- Zhang, W., Cao, B., Wang, D., Ma, T., Xia, H., Yu, D., 2016. Influence of wastewater sludge treatment using combined peroxyacetic acid oxidation and inorganic coagulants re-flocculation on characteristics of extracellular polymeric substances (EPS). *Water Res.* 88, 728–739. <https://doi.org/10.1016/j.watres.2015.10.049>.
- Zhao, Y., Yang, Q.S., Yang, S., Zhao, H.M., Duan, Q.S., Yang, Y.X., Qin, X.D., 2014. Effects of biogas slurry pretreatment on germination and seedling growth of *Vicia faba* L. *Adv. Mater. Res.* 955–959, 208–212. <https://doi.org/10.4028/www.scientific.net/AMR.955-959.208>.
- Zhou, Q., Li, X., Lin, Y., Yang, C., Tang, W., Wu, S., Li, D., Lou, W., 2019. Effects of copper ions on removal of nutrients from swine wastewater and on release of dissolved organic matter in duckweed systems. *Water Res.* 158, 171–181. <https://doi.org/10.1016/j.watres.2019.04.036>.